CIS Chem Mat 2009

DATASET · JUNE 2013

READS
341

6 AUTHORS, INCLUDING:

T. Jean Daou
Université de Haute-Alsace
68 PUBLICATIONS **1,162** CITATIONS
SEE PROFILE

Isabelle Texier
Atomic Energy and Alternative Energies Co…
79 PUBLICATIONS **1,356** CITATIONS
SEE PROFILE

Tran Thi Kim Chi
Vietnam Academy of Science and Technol…
34 PUBLICATIONS **362** CITATIONS
SEE PROFILE

Nguyen Quang Liem
Institute of Materials Science (IMS), VAST
84 PUBLICATIONS **765** CITATIONS
SEE PROFILE

Highly Luminescent $CuInS_2$/ZnS Core/Shell Nanocrystals: Cadmium-Free Quantum Dots for In Vivo Imaging

Liang Li,[†] T. Jean Daou,[‡,§] Isabelle Texier,[‡] Tran Thi Kim Chi,[||] Nguyen Quang Liem,[||] and Peter Reiss*[,†]

DSM/INAC/SPrAM (UMR 5819 CEA-CNRS-UJF), Laboratoire d'Electronique Moléculaire, Organique et Hybride, and DRT/LETI/DTBS/LFCM, CEA Grenoble, 17 rue des Martyrs, 38054 Grenoble cedex 9, France, Equipe Matériaux à Porosité Contrôlée, Institut de Science des Matériaux de Mulhouse (IS2M), LRC CNRS 7228−UHA−ENSCMu, 3 rue Alfred Werner, F-68093 Mulhouse Cedex, France, and Institute of Materials Science (IMS), Vietnam Academy of Science and Technology (VAST), 18 Hoang Quoc Viet, Cau Giay, Hanoi, Vietnam

Received January 13, 2009. Revised Manuscript Received April 17, 2009

Strongly luminescent $CuInS_2$/ZnS core/shell nanocrystals were synthesized from copper iodide, indium acetate, zinc stearate, and dodecanethiol as starting compounds in octadecene solvent. The as-prepared core/shell nanocrystals exhibit a low size distribution (<10%), and present photoluminescence in the range of 550−815 nm with a maximum fluorescence quantum yield (QY) of 60%. Time-resolved fluorescence spectroscopy revealed that the lifetimes of the different spectral components are on the order of hundreds of nanoseconds, indicating that donor−acceptor pair recombinations are at the origin of the observed emission bands. The $CuInS_2$/ZnS nanocrystals were subsequently transferred to the aqueous phase via surface ligand exchange with dihydrolipoic acid and used as fluorescent labels for in vivo imaging. After tail vein injection into nude mice, the biodistribution of the quantum dots was monitored during 24 h using fluorescence reflectance imaging.

Introduction

Semiconductor nanocrystals (NCs), also termed quantum dots (QDs), are of great interest for fundamental studies[1−3] and technical applications such as biomedical labeling, light-emitting diodes (LEDs), solar cells, lasers, and sensors.[4−8] II−VI and IV−VI semiconductors such as CdSe, CdTe, and PbSe and their alloys have been intensively studied in the form of size- and shape-controlled NCs during the past decade.[9−14] However, despite their appealing optical properties, the intrinsic toxicity of cadmium and lead sheds a doubt on the future applicability of these NCs, particularly in view of recent environmental regulations. Several Cd- and Pb-free alternative materials have been proposed, including III−V semiconductor NCs (e.g., InP) and transition-metal-doped ZnSe NCs.[15] Each of these systems has advantages and drawbacks in terms of tunability and purity of the emission color, fluorescence quantum yield (QY), lifetime, and photostability. In the particular case of in vivo biological labeling, absorption, and emission of the NCs within the near-infrared spectral window of 650−900 nm is required in order to minimize the light absorption/diffusion by molecules relevant to biological systems (water, hemoglobin, oxyhemoglobin).[16] NCs of low band gap semiconductors are needed to go to this spectral range, and therefore the in vivo studies implying QDs are limited to CdSe, CdTe, PbS and InAs based systems to date.[17−19]

Apart from binary II−VI and III−V compounds, multinary semiconductor NCs such as I−III−VI_2-type chalcopyrites

* Corresponding author. E-mail: peter.reiss@cea.fr. Fax: 33 438 78 51 13. Tel: 33 438 78 97 19.
† DSM/INAC/SPrAM (UMR 5819 CEA-CNRS-UJF), Laboratoire d'Electronique Moléculaire, Organique et Hybride, CEA Grenoble.
‡ DRT/LETI/DTBS/LFCM, CEA Grenoble.
§ LRC CNRS 7228−UHA−ENSCMu.
|| Vietnam Academy of Science and Technology.

(1) Brus, L. E. *J. Chem. Phys.* **1983**, *79*, 5566–5571.
(2) Alivisatos, A. P. *Science* **1996**, *271*, 933–937.
(3) Murray, C. B.; Norris, D. J.; Bawendi, M. G. *J. Am. Chem. Soc.* **1993**, *115*, 8706–8715.
(4) Bruchez, M., Jr.; Moronne, M.; Gin, P.; Weiss, S.; Alivisatos, A. P. *Science* **1998**, *281*, 2013–2016.
(5) Murray, C. B.; Kagan, C. R.; Bawendi, M. G. *Annu. Rev. Mater. Sci.* **2000**, *30*, 545–610.
(6) Chan, W. C. W.; Nie, S. *Science* **1998**, *281*, 2016–2018.
(7) Colvin, V. L.; Schlamp, M. C.; Alivisatos, A. P. *Nature* **1994**, *370*, 354.
(8) Klimov, V. I.; Mikhailovsky, A. A.; Xu, S.; Malko, A.; Hollingsworth, J. A.; Leatherdale, C. A.; Eisler, H. J.; Bawendi, M. G. *Science* **2000**, *290*, 314–317.
(9) Nazzal, A. Y.; Qu, L.; Peng, X.; Xiao, M. *Nano Lett.* **2003**, *3*, 819–822.
(10) Talapin, D. V.; Rogach, A. L.; Shevchenko, E. V.; Kornowski, A.; Haase, M.; Weller, H. *J. Am. Chem. Soc.* **2002**, *124*, 5782–5790.
(11) Yu, W. W.; Wang, Y. A.; Peng, X. *Chem. Mater.* **2003**, *15*, 4300–4308.
(12) Rogach, A. L.; Kornowski, A.; Gao, M.; Eychmüller, A.; Weller, H. *J. Phys. Chem.* **1999**, *103*, 3065–3069.
(13) Rogach, A. L.; Kornowski, A.; Kershaw, S. V.; Burt, M.; Harrison, M.; Eychmüller, A.; Weller, H. *Adv. Mater.* **1999**, *11*, 552–554.
(14) Peng, Z.; Peng, X. *J. Am. Chem. Soc.* **2001**, *123*, 183–184.
(15) Pradhan, N.; Goorskey, D.; Thessing, J.; Peng, X. *J. Am. Chem. Soc.* **2005**, *127*, 17586–17587.
(16) Klostranec, J. M.; Chan, W. C. *Adv. Mater.* **2006**, *18*, 1953.
(17) (a) Kim, S.; Lim, Y. T.; Soltesz, E. G.; DeGrand, A. M.; Lee, J.; Nakayama, A.; Parker, J. A.; Mihaljevic, T.; Laurence, R. G.; Dor, D. M.; Cohn, L. H.; Bawendi, M. G.; Frangioni, J. V. *Nat. Biotechnol.* **2004**, *22*, 93–97. (b) Zimmer, J. P.; Kim, S. W.; Ohnishi, S.; Tanaka, E.; Frangioni, J. V.; Bawendi, M. G. *J. Am. Chem. Soc.* **2006**, *128*, 2526–2527.
(18) Aharoni, A.; Mokari, T.; Popov, I.; Banin, U. *J. Am. Chem. Soc.* **2006**, *128*, 257.
(19) Xie, R.; Chen, K.; Chen, X.; Peng, X. *Nano Res.* **2008**, *1*, 457–464.

10.1021/cm900103b CCC: $40.75
Published on Web 05/11/2009

($CuInSe_2$, CISe; $CuInS_2$, CIS) offer an interesting alternative. They are direct semiconductors with band gaps of 1.05 eV (CISe) and 1.5 eV (CIS),[20] respectively, and provide high absorption coefficients and radiation stability. So far CIS and CISe NCs have mainly been studied for their high potential in solar energy conversion,[21−35] which has motivated the development of many synthetic approaches including solvothermal synthesis,[21−24] thermolysis,[25,26,34] photochemical decomposition,[27] and the hot-injection method.[28−33,35] An early example of a study of the photoluminescence of CISe NCs was reported by Malik et al.,[28] who modified the trioctylphosphine oxide (TOPO) based synthesis route which is widely applied for II−VI semiconductor QDs. Later, Castro and co-workers described the synthesis of CISe and CIS NCs via the decomposition of single-source precursors in the presence of a suitable ligand, and obtained luminescent CIS samples with a PL QY on the order of 5%.[25] Nakamura et al. successfully doped Zn ions into the CIS system, and varied their PL from 570 to 800 nm with a QY of 5%.[36] Although in the most recent reports on ternary systems ($AgInS_2$, CISe) higher QYs up to 25% have been reported,[37,38] these values are still significantly lower than those of II−VI semiconductor QDs (40−85%).

In this article, we provide a simple and reliable synthesis method for CIS-based NCs showing increased fluorescence QY and high photostability. In the two-step procedure, first CIS NCs were prepared in the noncoordinating solvent octadecene using copper iodide, indium acetate, myristic acid, and dodecanethiol. The latter compound has the double role of the sulfur source and the stabilizing ligand for the NC surface. The resulting NCs were subsequently overcoated with a ZnS shell using a mixture of zinc ethylxanthate and zinc stearate. During the shell growth, the PL QY strongly increased to values of 20−60%. In addition to absorption and PL spectroscopy, the optical properties of the obtained CIS/ZnS core/shell NCs were studied by means of time-resolved PL spectroscopy. The observed lifetimes of several hundreds of nanoseconds together with the comparably broad line width indicated that the emission bands originated from donor−acceptor pair recombinations rather than from excitonic emission. The last part of the article describes the transfer of the CIS/ZnS NCs to the aqueous phase by ligand exchange with dihydrolipoic acid and their subsequent application as fluorescent labels in in vivo biological imaging.

Experimental Section

Chemicals. Zinc stearate (90%) was purchased from Riedel de Haën, copper(I)iodide (99.995%) from Acros Organics. Indium(III)acetate ($In(OAc)_3$, 99.99%), 1-dodecanethiol (DDT, 97%), 1-octadecene (ODE, 90%), oleylamine (OA, 90%) and all other products were purchased from Sigma-Aldrich. Zinc ethylxanthate was prepared according to the method reported previously from zinc chloride and potassium ethylxanthogenate.[39]

Synthesis of CIS Core and CIS/ZnS Core/Shell NCs. The experimental parameters of a typical reaction are given. Values in brackets indicate the range of reaction temperature/time also explored and discussed. $In(OAc)_3$ (0.1 mmol) and CuI (0.1 mmol) were mixed with 1.0 mL (4.175 mmol) of DDT and 8 mL of ODE in a 50 mL three-neck flask under an inert atmosphere. The mixture was heated to 50−80 °C under a primary vacuum and magnetic stirring for 1 h, backfilled with Ar, and then heated to the reaction temperature of 230 °C (200−270 °C) with a rate of 150−200 K/min. The color of the reaction solution progressively changed from colorless to green, yellow, red, and finally dark brown. After keeping the mixture at the reaction temperature for 40 min (15−290 min), the heating source was removed and the NCs were isolated by adding 1 equiv. of a chloroform/methanol (1:1 vol:vol) mixture, precipitating with 10 equiv. of acetone, and centrifuging. The NCs could be redispersed in organic solvents such as hexanes, toluene, or chloroform. The precipitation/dispersion cycle was repeated at least twice in order to eliminate byproducts, unreacted precursors, and ODE.

The ZnS precursor solution was prepared by dissolving 0.8 mmol of zinc stearate in 3 mL of ODE and adding a solution of 0.1 mmol of zinc ethylxanthate in 100 μL of dimethylformamide (DMF) and 1 mL of toluene. Without intermediate purification step of the core NCs, the ZnS shell precursor solution was added dropwise by means of a syringe pump within 30 min to the CIS NCs containing reaction mixture at 230 °C. Purification of the core/shell NCs was carried out in the same way as described for the core NCs.

Transfer of the CIS/ZnS NCs to the Aqueous Phase. The phase transfer was achieved by replacing the initial surface ligands (dodecanethiol) with dihydrolipoic acid (DHLA) using the following exchange procedure. First, the NCs were precipitated using ethanol, followed by elimination of the ethanol phase and drying under reduced pressure. Dodecanethiol capping ligands were subsequently exchanged by suspending the sedimented precipitate in 40 μL of DHLA. The mixture was then heated to 70 °C for 2 h. After dilution

(20) Jaffe, J. E.; Zunger, A. *Phys. Rev. B* **1984**, *29*, 1882–1906.
(21) Xiao, J.; Xie, Y.; Xiong, Y.; Tang, R.; Qian, Y. T. *J. Mater. Chem.* **2001**, *11*, 1417.
(22) Li, B.; Xie, Y.; Huang, J.; Qian, Y. T. *Adv. Mater.* **1999**, *11*, 1456.
(23) Jiang, Y.; Wu, Y.; Mo, X.; Yu, W. C.; Xie, Y.; Qian, Y. T. *Inorg. Chem.* **2000**, *39*, 2964.
(24) Gou, X.; Cheng, F.; Shi, Y.; Zhang, L.; Peng, S.; Chen, J.; Shen, P. *J. Am. Chem. Soc.* **2006**, *128*, 7222.
(25) (a) Castro, S. L.; Bailey, S. G.; Raffaelle, R. P.; Banger, K. K.; Hepp, A. F. *Chem. Mater.* **2003**, *15*, 3142. (b) Castro, S. L.; Bailey, S. G.; Raffaelle, R. P.; Banger, K. K.; Hepp, A. F. *J. Phys. Chem. B* **2004**, *108*, 12429.
(26) Zhong, H.; Zhou, Y.; Ye, M.; He, Y.; Ye, J.; He, C.; Yang, C.; Li, Y. *Chem. Mater.* **2008**, *20*, 6434–6443.
(27) Nairn, J. J.; Shapiro, P. J.; Twamley, B.; Pounds, T.; von Wandruszka, R.; Fletcher, T. R.; Williams, M.; Wang, C.; Norton, M. G. *Nano Lett.* **2006**, *6*, 1218–1223.
(28) Malik, M. A.; O'Brien, P.; Revaprasadu, N. *Adv. Mater.* **1999**, *11*, 1441–1444.
(29) Zhong, H.; Li, Y.; Ye, M.; Zhu, Z.; Zhou, Y.; Yang, C.; Li, Y. *Nanotechnology* **2007**, *18*, 025602.
(30) Pan, D. C.; An, L. J.; Sun, Z. M.; Hou, W.; Yang, Y.; Yang, Z. Z.; Lu, Y. F. *J. Am. Chem. Soc.* **2008**, *130*, 5620–5621.
(31) Guo, Q. J.; Kim, S. J.; Kar, M.; Shafarman, W. N.; Birkmire, R. W.; Stach, E. A.; Agrawal, R.; Hillhouse, H. W. *Nano Lett.* **2008**, *8*, 2982–2987.
(32) Banger, K. K.; Jin, M. H.-C.; Harris, J. D.; Fanwick, P. E.; Hepp, A. F. *Inorg. Chem.* **2003**, *42*, 7713–7715.
(33) Arici, E.; Sariciftci, N. S.; Meissner, D. *Adv. Funct. Mater.* **2003**, *13*, 165–171.
(34) Panthani, M. G.; Akhavan, V.; Goodfellow, B.; Schmidtke, J. P.; Dunn, L.; Dodabalapur, A.; Barbara, P. F.; Korgel, B. A. *J. Am. Chem. Soc.* **2008**, *130*, 16770–16777.
(35) Tang, J.; Hinds, S.; Kelley, S. O.; Sargent, E. H. *Chem. Mater.* **2008**, *20*, 6906–6910.
(36) Nakamura, H.; Kato, W.; Uehara, M.; Nose, K.; Omata, T.; Matsuo, S. O.; Miyazaki, M.; Maeda, H. *Chem. Mater.* **2006**, *18*, 3330–3335.
(37) Torimoto, T.; Adachi, T.; Okazaki, K.-i.; Sakuraoka, M.; Shibayama, T.; Ohtani, B.; Kudo, A.; Kuwabata, S. *J. Am. Chem. Soc.* **2007**, *129*, 12388–12389.
(38) Allen, P. M.; Bawendi, M. G. *J. Am. Chem. Soc.* **2008**, *130*, 9240–9241.
(39) Protière, M.; Reiss, P. *Small* **2007**, *3*, 399–403.

with 1 mL of DMF, deprotonation of the terminal lipoic acid carboxylate groups was carried out by slowly adding excess potassium tert-butoxide. The resulting precipitate was then redispersed in sterilized buffer (PBS 1X). Purification of the QDs after ligand exchange was achieved using NAP-5 size exclusion columns from GE-Biosciences. Finally, the NCs were stabilized in the buffer by adding a small amount of DHLA. The functionalized NCs were stable for 1 month in PBS, pH 7.4, under ambient conditions without detectable flocculation or modification of their fluorescence properties.

Intravenous Injection of the CIS/ZnS NCs into Mice and Determination of the Biodistribution. Two-hundred microliters of the aqueous dispersion of CIS/ZnS NCs prepared as described above (equivalent to 6.5×10^{16} to 1.3×10^{17} Cu atoms as quantified by inductively coupled plasma mass spectrometry (ICP-MS)) were sterilized by 0.22 μm filtration and injected intravenously into the tail vein of healthy nude female mice aged 6−8 weeks (Janvier, France), anesthetized with isoflurane (1.5% in air) for the duration of the experiment. All animal experiments were performed in agreement with the EEC guidelines and the "Principles of laboratory animal care" (NIH publication 86−23 revised 1985).

Optical Characterization. UV−vis absorption spectra were recorded on a HP 8452A spectrometer, photoluminescence spectra on a Hitachi F-4500 spectrofluorometer. Values of the absolute fluorescence quantum yield (QY) were determined by comparison of the integrated fluorescence intensity of a NC's dispersion with that of a standard of known QY (Rhodamine 6G in ethanol, QY = 95%). The absorbance of the NC's dispersion was below 0.1 at the higher-energy shoulder close to the absorption onset. The absorbance of the standard solution was adjusted to be identical to that of the NCs' dispersion at the excitation wavelength (470 nm). The QY of each sample was determined for at least three different concentrations.

For time-resolved photoluminescence (TRPL) experiments, the 337.1 nm (equivalent to 3.677 eV) light from a pulsed nitrogen laser (~1 ns pulse duration, repetition rate of 30 pulses per second) was used as the excitation source. The excitation power density was set around 50 kW/cm^2 on the sample surface by using the combination of neutral density filters. The PL signal was dispersed by a double grating monochromator (Jobin-Yvon HRD1) and detected by a fast and sensitive photomultiplier (H7313 Hamamatsu). At each wavelength of the spectrum measured, the electrical signal pulse like a luminescence-decay curve was recorded. Then, by extraction of the PL data as a function of the delay time from the excitation moment, the TRPL spectra could be reproduced. Averaging the multipulses at each spectral point by using a 1.5 GHz digital oscilloscope (LeCroy 9362) significantly improved the signal-to-noise ratio.

Photostability. The stability of the samples against photo-oxidation was assessed by placing them into quartz cuvettes with half of the volume being filled with air and continuously irradiating them with a UV lamp (365 nm, distance lamp-sample: 2.5 cm, irradiation power at the sample surface approximately 1−3 mW). The photodegradation was monitored by taking UV−vis and PL spectra at certain time intervals.

Size and Structural Characterization. Transmission electron microscopy (TEM) images of the synthesized CIS and CIS/ZnS NCs were obtained with a JEOL 4000 EX microscope operated at 400 kV. The NCs were drop-cast from a diluted dispersion in toluene onto a thin holey carbon film supported by a copper grid (Ted Pella). The hydrodynamic diameter of the water-soluble NCs dispersed in PBS 1X was measured by dynamic light scattering (DLS), using a Malvern Zeta Sizer (NanoZS). Powder X-ray diffraction (XRD) was performed in the reflection geometry using a Philips X'PERT diffractometer with Co Kα radiation (wavelength 1.789 Å). EDX analyses of samples drop-cast on Si/SiO_2 substrates were carried out with a JEOL JSM-840A scanning electron microscope equipped with an Oxford Instruments energy-dispersive X-ray analyzer.

Imaging System. A homemade system, adapted from the commercially available Aequoria system from Hamamatsu, was used. It is made of a dark box equipped with a mouse-body temperature controller and a gas anesthesia device. The excitation device is composed of 10 LEDS emitting at 633 nm (adapted from the LuxiFlux device available from Hamamatsu) and equipped with interference band-pass filters (633BP10 nm from Schott) for a light illumination power of 15 μW cm^{-2}. The filtered fluorescence signal (filter RG665 from Schott) was detected by a cooled CCD Camera (Orca II BT 512 G, Hamamatsu) placed at 160 mm from the imaging field, with an exposure time of 500 ms, the gain of the camera was set at medium and the binning was 1 × 1. The Wasabi software (Hamamatsu) was used to drive the setup and for image processing. Outside of the dark box an anaesthetized mouse (Female NMRI nude mice, 5−6 weeks old, purchased from Janvier) was placed on a warm plate (37.5 °C) connected to an anesthesia mask (isoflurane/air 1.5%). Two hundred microliters of particles in PBS 1X buffer were injected intravenously (IV) via the tail vein and the mouse was imaged at each desired time point. Fluorescence images can be superimposed on the black and white pictures for better localization of the fluorescence signal. Semiquantitative data can be obtained by drawing regions of interest (ROI) on the area to be quantified. The results are expressed as a number of relative light units per pixel (RLU/pix).

Results and Discussion

Absorption and Photoluminescence Properties of the Core CIS NCs. The evolution of the absorption and emission spectra of CIS NCs during the synthesis at 200 °C is shown in Figure 1. The onset of the absorption spectra underwent a bathochromic shift from 550 to 740 nm with reaction time, indicating the growth of small CIS NCs in the quantum confinement regime. The observed shoulder in the absorption spectra is assigned to the excitonic transition of the CIS NCs. In the first minutes of the reaction, only a weak emission peak at low energy (~800−820 nm) could be detected; after 20 min, a stronger luminescence signal was observed (Figure 1b).

The spectrum is composed of three peaks including a high-energy peak at 660 nm (strongest peak), a lower-energy band located at 713 nm, and a weak peak at 806 nm. With prolonged reflux time, the overall fluorescence intensity became stronger. The second peak increased faster than the first one, and gradually became the maximum peak after 60 min. The first peak shifted from 660 to 680 nm at the same time, whereas the two lower-energy signals showed a stable spectral position. Further heating caused a continued shift of the first peak, leading to its superposition with the second one after approximately 130 min. The first and second peak vanished during the subsequent heating. After 290 min, only the lowest-energy peak at 810−820 nm remained, which was also quenched if heating was continued. In addition to the reaction time, the reaction temperature was varied in a range of 200−300 °C to study its influence on the growth of CIS NCs. Higher temperatures resulted in an accelerated growth and yielded larger-sized NCs at identical reaction times because of the faster decomposition of DDT. However, if

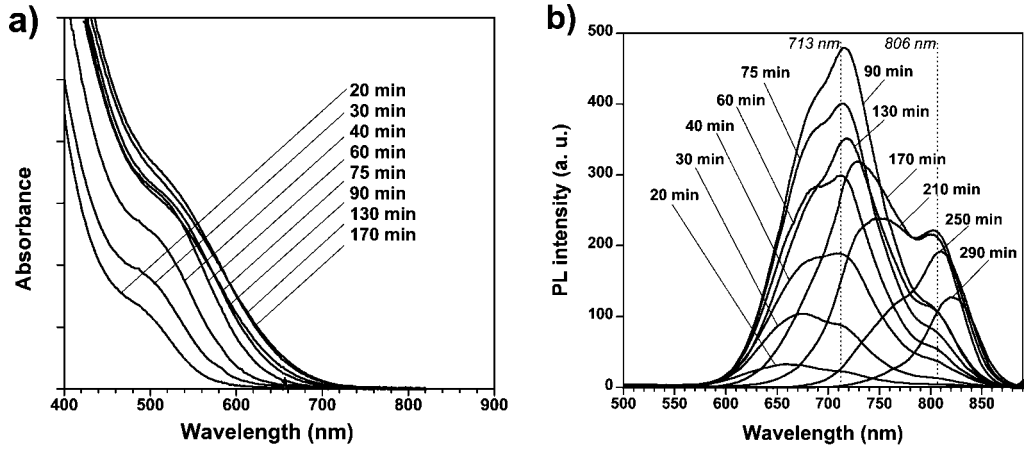

Figure 1. Temporal evolution of the (a) absorption and (b) photoluminescence (excitation wavelength: 470 nm) spectra of CIS NCs synthesized at 200 °C.

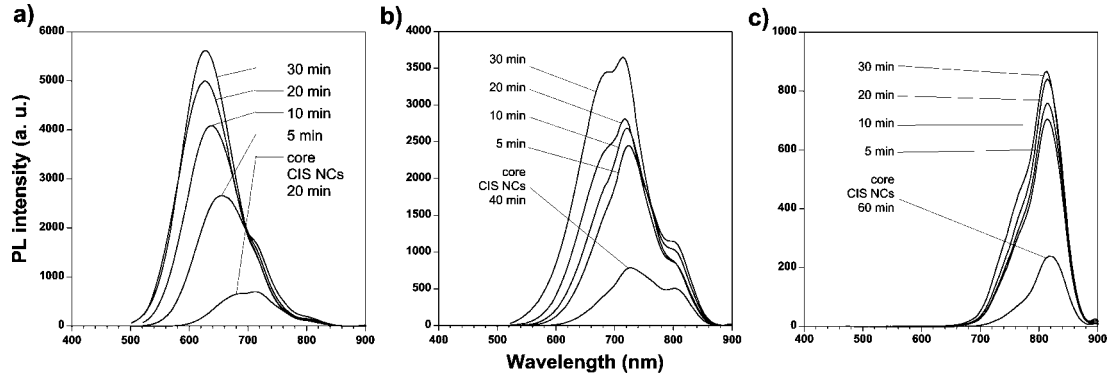

Figure 2. Evolution of the PL spectra of different sized CIS NCs during the growth of a ZnS shell. (a) CIS20M, (b) CIS40 M, and (c) CIS60 M were synthesized at 230 °C.

the temperature was too high (∼290−300 °C) or the reflux time too long (≫1 h), precipitation of the NCs within the reaction mixture occurred. The observed precipitation can be attributed to the fact that DDT acts as both the sulfur precursor and the stabilizing ligand during the reaction. Therefore, its complete decomposition results in a destabilization of the colloids. We found that adding a small amount of oleylamine (∼100−200 μL) in the beginning of the reaction prevented from precipitation, but led, on the other hand, to quenching of the fluorescence of the core CIS NCs.

The influence of the nature of the stabilizing ligand/sulfur source on the growth of the CIS NCs was also investigated. The use of alkylthiols, already proposed by Zhong et al.,[26] turned out to be essential for the successful synthesis of CIS NCs, while amines (e.g., oleylamine) or fatty acids (e.g., myristic acid or oleic acid) led to the formation of aggregated products, in accordance with the observations of Castro et al.[25] When DDT was replaced by 1-octadecanethiol (ODT), the growth of CIS NCs required higher temperatures because of the higher decomposition temperature of ODT. Alternatively, thio-urea, quickly injected into the reaction mixture at high temperature, could be used as the sulfur source in combination with alkylthiol stabilizing ligands. In all cases, the resulting CIS NCs showed very similar optical properties as those obtained with DDT as both the stabilizer and sulfur source.

It has been demonstrated in earlier works that a broad size distribution cannot account for the observed broad and multiple peaks in the PL spectra of colloidal CIS NCs.[25,34] We used size-selective precipitation by means of the dropwise addition of ethanol to a dispersion of CIS NCs in hexane to reduce their size distribution.[3] Although the positions and the relative intensity of the peaks of the resulting fractions differ slightly with respect to the crude sample, the number of the peaks did not change and only slight narrowing of the overall spectra was observed.

Overcoating of the CIS NCs with a ZnS Shell. The fluorescence quantum yield (QY) and photostability of binary semiconductor NCs (e.g., CdSe) have been significantly improved by means of the growth of a shell of a higher band gap material.[40−43] Although similar attempts for the surface passivation of CIS NCs appeared in the recent literature,[26,44] none of these works reported a fluorescence QY exceeding 10%. We chose ZnS as the shell material for different reasons: (i) it is a large band gap (3.6 eV) semiconductor exhibiting a type I band alignment with CIS; (ii) the crystal structure of CIS can be described as a derivative of the zinc blende structure, in which the zinc positions are occupied

(40) Hines, M. A.; Guyot-Sionnest, P. *J. Phys. Chem.* **1996**, *100*, 468–471.
(41) Dabbousi, B. O.; Rodriguez-Viejo, J.; Mikulec, F. V.; Heine, J. R.; Mattoussi, H.; Ober, R.; Jensen, K. F.; Bawendi, M. G. *J. Phys. Chem. B* **1997**, *101*, 9463–9475.
(42) Peng, X.; Schlamp, M. C.; Kadavanich, A. V.; Alivisatos, A. P. *J. Am. Chem. Soc.* **1997**, *119*, 7019–7029.
(43) Reiss, P.; Bleuse, J.; Pron, A. *Nano Lett.* **2002**, *2*, 781–784.
(44) Kuo, K.-T.; Chen, S.-Y.; Cheng, B.-M.; Lin, C.-C. *Thin Solid Films* **2008**, *517*, 1257–1261.

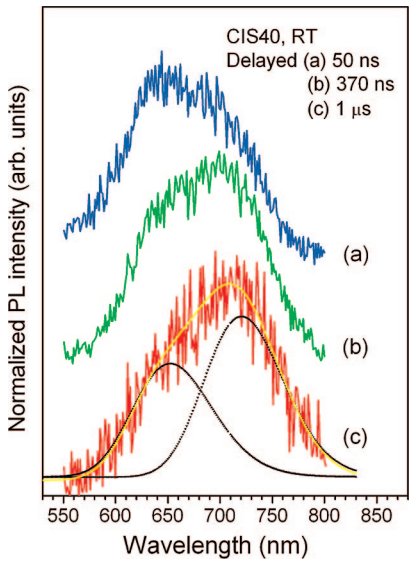

Figure 3. TRPL spectra of CIS40M/ZnS at different delay times as indicated. Two Gaussian spectral components, peaking at ~650 and ~720 nm, from deconvolution of the 1 μs delayed spectrum (bottom).

by Cu and In, respectively, and the lattice mismatch between CIS and ZnS is relatively low (2−3%); (iii) ZnS is a promising shell material because of its chemical stability and nontoxic character. As can be seen in Figure 2, the overgrowth of different sized CIS core NCs resulted in a strong enhancement of the PL intensity. The QY of the samples increased from 8 to 60% (CIS20M, reaction time 20 min), 8 to 41% (CIS40M, reaction time 40 min) and 4 to 12% (CIS60M, reaction time 60 min), respectively. These values are the highest reported for ternary chalcopyrite NCs to date, and open up the way for the use of CIS NCs in many applications such as light-emitting devices or fluorescent biological labeling and sensing. Interestingly, depending on the predominant spectral components of the core NCs, different spectral components can be increased upon ZnS shell growth. For the smallest NCs (reaction time 20 min, CIS20M, Figure 2a), the size-dependent peak at the shortest wavelength exhibits a strongly increased intensity accompanied by a pronounced blue-shift in the initial stages of shell growth. Taking into account the relatively low temperature of 230 °C during the ZnS deposition, this blue-shift most probably does not originate from the diffusion of Zn into the CIS core NCs, but is rather related to surface reconstruction. In the case of bigger core CIS NCs (CIS40M, CIS60M), either one or both of the peaks showed increased intensity at essentially invariant wavelength in the near-infrared region (around 710 and 815 nm) upon the ZnS shell growth (samples B and C in Figure 2a). Therefore, it can be concluded that the underlying optical transitions are not related to surface defects, as otherwise these peaks should vanish during the surface passivation step.

Time-Resolved Photoluminescence Spectroscopy of the CIS/ZnS NCs. To further elucidate the emission properties of the prepared CIS/ZnS NCs, we carried out time-resolved PL measurements. Figure 3 shows the PL spectra at different delay times (indicated in the figure) of the sample CIS40 M after ZnS shell growth. Just after the excitation, the PL spectrum shows one broad and asymmetric peak at ~640 nm. It should be noted that the zero-delayed TRPL spectrum has a markedly different shape as compared to that taken from the steady-state PL measurement (Figure 2b). Varying the delay times clearly reveals two emission bands with different decays. We carried out the deconvolution of the 1 μs delayed spectrum showing two spectral components. The one located at shorter wavelength (~650 nm) decayed with shorter time, estimated to be of 280 ns; the other located at longer wavelength (~720 nm) decayed by 370 ns. The latter evolved then to be the maximal peak in the steady-state PL spectrum recorded with a certain accumulation time (typically a few seconds).

The decay times for both spectral components, namely the 650 and 720 nm bands, are very long, which rules out the assignments of these bands to originate from excitonic-related transitions. By means of the deconvolution of the TRPL spectra to get exact spectral components, we have determined the red-shift of both the 650 and 720 nm bands with the delay time. This behavior is characteristic for the donor−acceptor pair recombination as a consequence of the contribution of the Coulomb energy, which decreases with increasing separation distance between donors and acceptors. The peak difference of 70 nm (~180 meV) between the two mentioned bands is rather large if compared to the energy level diagram proposed in ref 22. The detailed analyses of the TRPL behavior and of the activation energy corresponding to each emission band in CIS NCs are under progress and will be reported elsewhere. Being a ternary compound, CIS naturally contains more lattice imperfections than, for example, binary II−VI semiconductors. These defects act as potential fluctuations to localize carriers, consequently causing long lifetimes for the relevant transitions. On the other hand, this feature is very appealing for biological labeling, as it allows for time-resolved imaging. In this method, an appropriate delay time between the excitation pulse and the fluorescence detection is used to eliminate the background luminescence from the organic environment. The latter normally gives a strong signal in the first tens of nanoseconds after the excitation. In comparison with the II−VI semiconductor quantum dots actually used in bioimaging, such as CdSe and CdTe, the decay time of the PL from CIS NCs is much longer, enabling easier performance of time-resolved bioimaging.

Structural Characterization. Structural characterization was carried out by means of powder X-ray diffraction. Figure 4a shows the obtained diffraction pattern from the CIS samples synthesized at two temperatures, which exhibit the characteristic peaks of Roquesite. No mixture of different phases but only the peaks of the tetragonal CIS structure are observed. EDX analyses confirmed these results (Figure 4b): An equimolar Cu:In ratio is observed ($Cu_{21}In_{21}S_{58}$), whereas the sulfur content increases with respect to the expected value because DDT acts as the surface ligand. The XRD peaks are narrower for the sample produced at higher synthesis temperature, confirming that larger NCs were formed. After the sample was coated with the ZnS shell, all peaks exhibited a notable shift to larger angles, closer to the characteristic peak positions of bulk cubic ZnS. A similar behavior has been observed for other core/shell systems, such as CdSe/ZnS and CdSe/CdS.[41,42]

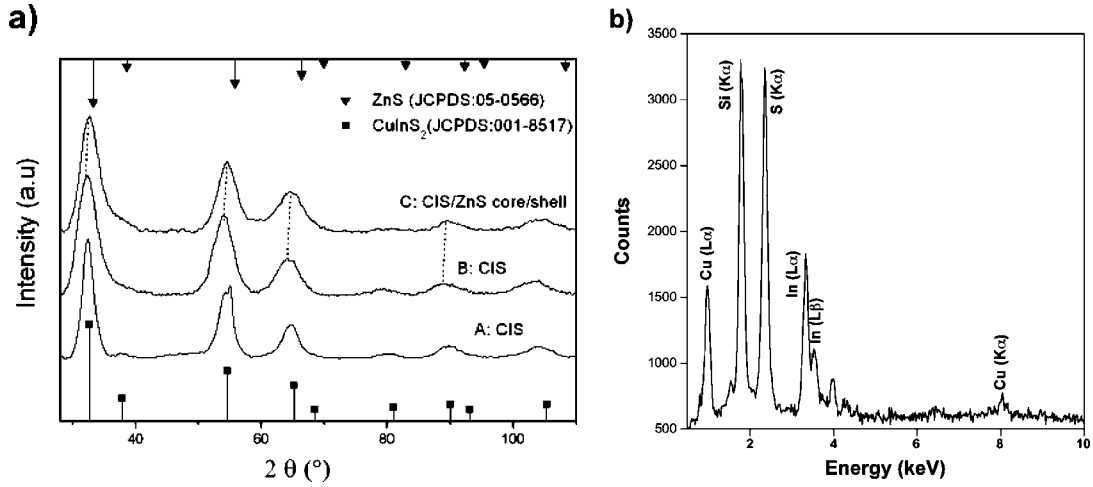

Figure 4. (a) XRD patterns of two different sized samples of CIS NCs: A, synthesized at 270 °C, 30 min; B, synthesized at 230 °C, 40 min; C, CIS/ZnS core/shell NCs obtained using sample B as core NCs. The diffraction patterns of bulk CIS and ZnS are indicated for comparison. (b) EDX analysis of the obtained CIS NCs (sample B).

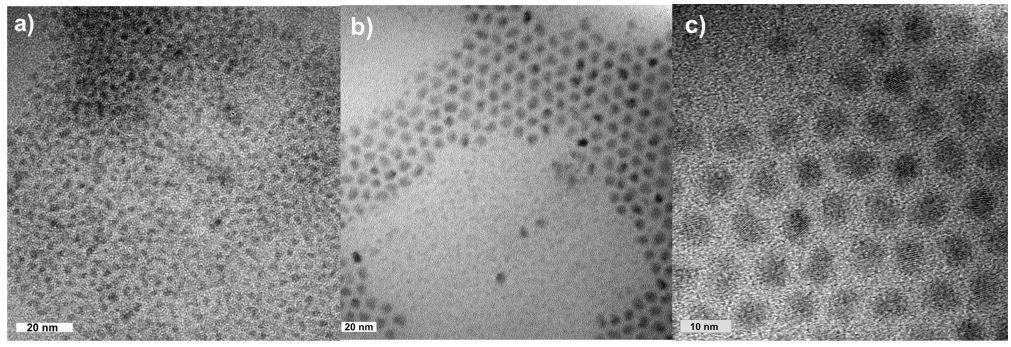

Figure 5. TEM images of (a) CIS core NCs (230 °C/40 min) and (b, c) the corresponding CIS/ZnS NCs at different magnifications.

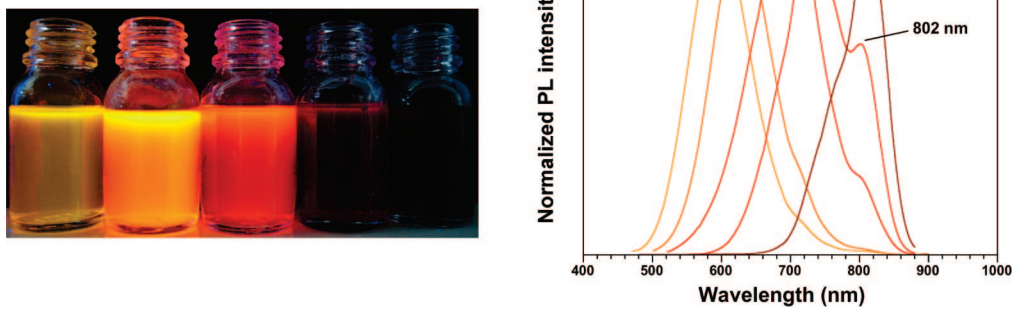

Figure 6. (a) Photograph of different sized CIS/ZnS NCs under UV light (core diameter around 2−4 nm from left to right). (b) Corresponding PL spectra (excitation at 470 nm).

Figure 5 shows the TEM images corresponding to the samples B and C in Figure 6. A strong increase in size from approximately 3 nm to around 7 nm can be observed upon shell growth. The CIS/ZnS core/shell NCs, containing roughly 5−6 ZnS monolayers, exhibit a similar size distribution as the core-alone NCs. The thick ZnS shell not only dramatically decreased the surface defects and increased the fluorescence efficiency but also yielded a highly photostable structure. Under continuous UV irradiation in the presence of oxygen, the CIS/ZnS NCs exhibited a similar evolution of the PL intensity as high quality CdSe/CdS/ZnS core/shell/shell NCs, which are known to be a very photostable system.[45]

Figure 6 shows a series of different sized CIS/ZnS core/shell NCs with emission from the visible to the near-infrared range. Even though the rather broad emission line width on the order of 100 nm is a drawback with respect to binary II−VI or III−V quantum dots, their high PL QY and good

(45) Talapin, D. V.; Mekis, I.; Gotzinger, S.; Kornowski, A.; Benson, O.; Weller, H. *J. Phys. Chem. B* **2004**, *108*, 18826–18831.

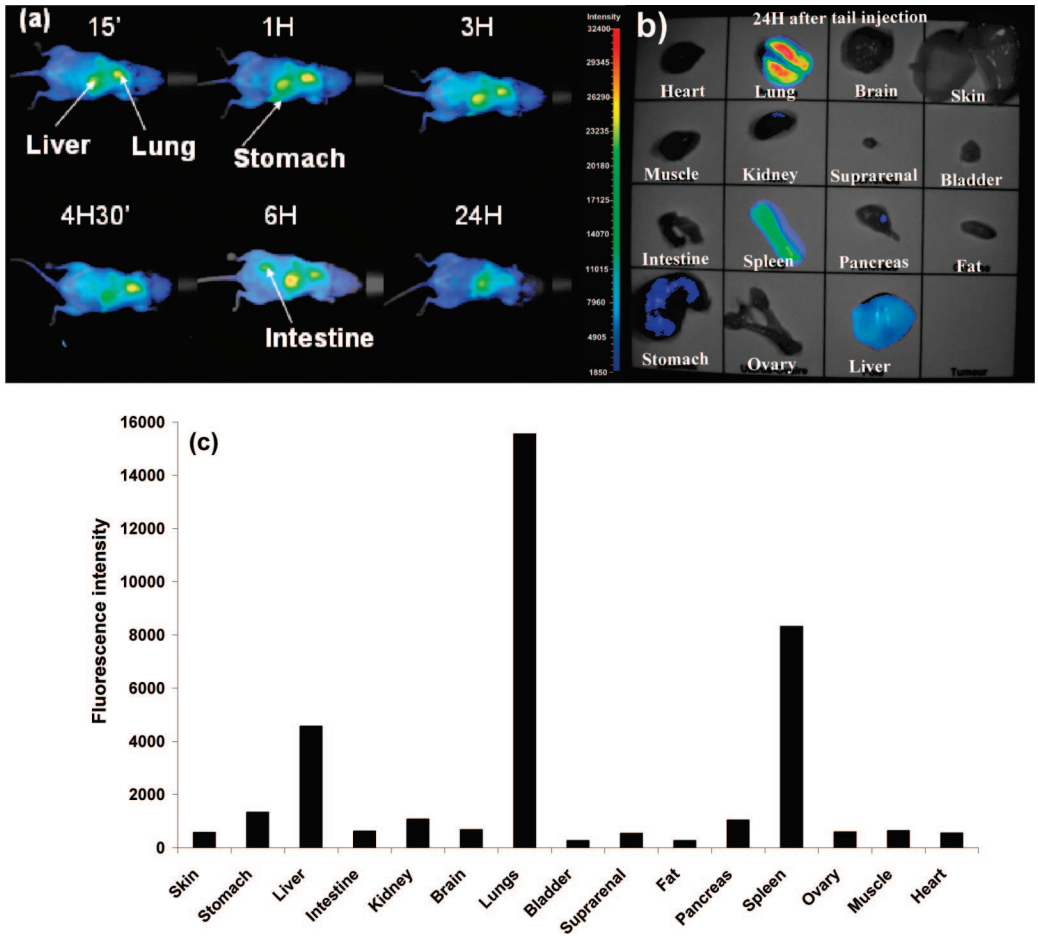

Figure 7. (a) Fluorescence images (excitation wavelength 633 nm) showing the temporal evolution of the biodistribution of the CIS/ZnS NCs injected intravenously into the tail of a healthy nude mouse (eq 6.5×10^{16} to 1.3×10^{17} copper atoms). The integration time is 200 ms and the contrast has been set between 1850 and 32400. (b) Fluorescence images of the different parts of the mouse after dissection. (c) Biodistribution and tissue fluorescence of the CIS/ZnS NCs, 24 h after tail vein administration.

photostability in combination with the absence of toxic elements such as Cd, Pb, or As, provide distinct advantages for potential applications. In particular, CIS/ZnS NCs are of special interest for in vivo biological imaging as this application requires the absorption and the emission of light by the probes in a spectral window of 650−900 nm in order to minimize light absorption and scattering by water and (oxy-)hemoglobin.[46] In the last part of this article, we will describe for the first time the application of chalcopyrite based NCs as fluorescent probes in in vivo experiments.

In Vivo Imaging Using CIS/ZnS NCs. For these experiments, CIS/ZnS NCs emitting in the range of 650−750 nm have been transferred to the aqueous phase (buffer PBS 1X) via ligand exchange with dihydrolipoic acid (cf. Experimental Section).[47] Upon phase transfer, because of the efficient surface passivation by the ZnS shell, only a slight decrease in the PL QY to 70−80% of the initial value was observed. The absence of aggregates has been confirmed by means of dynamic light scattering, yielding a hydrodynamic diameter of 17 ± 3 nm after ligand exchange, which indicates the presence of individual nanoparticles. The increase in the hydrodynamic diameter with respect to the TEM diameter (7 nm) in association with the use of dihydrolipoic acid (DHLA) providing an anionic surface coating is in accordance with the observations of Choi et al.[48] Purely anionic or cationic surface coatings led to hydrodynamic diameters >15 nm for NCs of a TEM (inorganic) diameter on the order of 5 nm because of the adsorption of serum proteins. In the present case (absence of serum proteins), the diameter increase is attributed to the formation of an ionic double layer around the negatively charged NCs in the PBS 1X buffer. The concentration of the QDs in aqueous solution has been determined after digestion of the NCs with 65% nitric acid, and the constituting elements have been analyzed by inductively coupled plasma mass spectrometry (ICP-MS). Subsequently, 200 μL of the aqueous QDs containing solution, corresponding to 6.5×10^{16} to 1.3×10^{17} copper atoms, have been injected intravenously (IV) into the tail of nude female mice 6−8 weeks of age. The mice have been imaged by fluorescence reflectance imaging (FRI) in order to determine the biodistribution of the QDs at different time points. Animals were kept under general anesthesia (isoflurane) for a few minutes for the QD injection and image

(46) Weissleder, R. *Nat. Biotechnol.* **2001**, *19*, 316–317.
(47) Uyeda, H. T.; Medintz, I. L.; Jaiswal, J. K.; Simon, S. M.; Mattoussi, H. *J. Am. Chem. Soc.* **2005**, *127*, 3870–3878.
(48) Soo Choi, H.; Liu, W.; Misra, P.; Tanaka, E.; Zimmer, J. P.; Itty Ipe, B.; Bawendi, M. G.; Frangioni, J. V. *Nat. Biotechnol.* **2007**, *25*, 1165–1170.

acquisitions. Figure 7 shows the evolution during 24 h of the fluorescence signal arising from the injected CIS/ZnS QDs. Throughout the observation time, no modification of the vital functions of the mouse could be detected and only negligible fluorescence fading was observed. Fifteen minutes after injection, the NCs accumulate essentially in the liver, spleen, and lungs. The fluorescence signal detected in the stomach is identical to that of a healthy Nude mouse without injection and attributed to the feed.[49] The noninvasive in vivo observations have been confirmed after subsequent dissection of the animal and analysis of the different organs 24 h after injection (Figure 9). Lungs are one of the blood first-pass organs after IV injection, and act as a filter (the smallest capillaries in mice have a diameter of approximately 3 μm). Liver and spleen, organs from the reticulo-endothelial system (RES), are known for their important uptake of nanoparticles, especially whenever these have been covered by circulating plasma opsonins.[50] DHLA-coated NCs bear negative charges at their surface, which should favor opsonin binding and therefore possibly formation of aggregates in vivo and RES uptake. Although these preliminary results already demonstrate the feasibility of in vivo imaging with CIS/ZnS QDs, we currently investigate the use of PEG-modified DHLA for the aqueous phase transfer, which should strongly reduce charge-induced nonspecific binding.

Conclusion

We described the synthesis of highly luminescent CIS/ZnS core/shell NCs, using easy-to-handle and low-cost reactants in a heating-up approach. Although further work is needed to investigate in more details the nature of the optical transitions at the origin of the observed emission bands, we already demonstrated the interest of these NCs as fluorescent probes for in vivo biological imaging. In this context, CIS/ZnS NCs combine several appealing features: their emission can be tuned in the near-infrared spectral region (650−830 nm), the ZnS shell provides comparably high quantum yields and photostability, and the relatively long lifetimes on the order of several hundreds of nanoseconds allows for time-resolved imaging and elimination of the background fluorescence from the biological environment. Finally, CIS/ZnS NCs are the first example of QDs to be applied in in vivo imaging that do not contain any toxic ions (e.g., Cd, Te, As, Pb). Their biodistribution could be monitored by fluorescence reflectance imaging over 24 h. The dihydrolipoic acid coating facilitates further surface functionalization with furtivity agents and targeting ligands (e.g., antibodies, peptides, saccharides), opening up the way to direct the NCs toward the zone of interest for visualization, such as for example tumors.

Acknowledgment. We thank Véronique Josserand and Mélanie Guidetti (Imaging Platform Floralis, Institut Albert Bonniot, Grenoble) for the animal handling and experiments. We acknowledge financial support from the Commissariat à l'Energie Atomique through the "Technologies pour la santé" program (TIMOMA2) and the French National Research Agency (ANR) through Carnot funding and the PNANO program (SYNERGIE project). N.Q.L. thanks the National Program on Basic Research in Natural Science (MOST Vietnam) for financial support.

CM900103B

(49) Daou, T. J.; Li, L.; Reiss, P.; Josserand, V.; Texier, I. *Langmuir* **2009**, *25*, 3040–3044.
(50) Couvreur, P.; Vauthier, C. *Pharm. Res.* **2006**, *23* (7), 1417–1450.